Impact of Common Sea Surface Temperature Anomalies on Global Drought and Pluvial Frequency

KIRSTEN L. FINDELL AND THOMAS L. DELWORTH

Geophysical Fluid Dynamics Laboratory, Princeton, New Jersey

(Manuscript received 27 March 2009, in final form 24 August 2009)

ABSTRACT

Climate model simulations run as part of the Climate Variability and Predictability (CLIVAR) Drought Working Group initiative were analyzed to determine the impact of three patterns of sea surface temperature (SST) anomalies on drought and pluvial frequency and intensity around the world. The three SST forcing patterns include a global pattern similar to the background warming trend, a pattern in the Pacific, and a pattern in the Atlantic. Five different global atmospheric models were forced by fixed SSTs to test the impact of these SST anomalies on droughts and pluvials relative to a climatologically forced control run.

The five models generally yield similar results in the locations of drought and pluvial frequency changes throughout the annual cycle in response to each given SST pattern. In all of the simulations, areas with an increase in the mean drought (pluvial) conditions tend to also show an increase in the frequency of drought (pluvial) events. Additionally, areas with more frequent extreme events also tend to show higher intensity extremes. The cold Pacific anomaly increases drought occurrence in the United States and southern South America and increases pluvials in Central America and northern and central South America. The cold Atlantic anomaly increases drought occurrence in southern Central America, northern South America, and central Africa and increases pluvials in central South America. The warm Pacific and Atlantic anomalies generally lead to reversals of the drought and pluvial increases described with the corresponding cold anomalies. More modest impacts are seen in other parts of the world. The impact of the trend pattern is generally more modest than that of the two other anomaly patterns.

1. Introduction

Droughts and floods are both potentially devastating events with serious implications for individuals, ecosystems, and societies. The human need to understand the causes of these events is underscored by the wide array of research on these topics spanning many decades. Despite these efforts, much work remains. The Climate Variability and Predictability (CLIVAR) Drought Working Group was established ''to facilitate progress on the understanding and prediction of long-term (multiyear) drought over North America and other drought-prone regions of the world, including an assessment of the impact of global change on drought processes'' (U.S. CLIVAR Drought Working Group Prospectus, 12 December 2006). From this directive, a multimodel comparison project was initiated, in which all the participating models were forced with the same set of three large-scale patterns of sea surface temperature (SST) anomalies. The goal of the project was to assess the role of these commonly occurring SST patterns in driving and/or exacerbating drought.

The goal of this paper is to document the impact of the three primary SST patterns on drought and pluvial frequency and intensity around the world throughout the annual cycle, as determined by the multimodel mean of these experiments. The dominance of the Pacific forcing stands out in these results, with secondary yet notable impacts forced by the North Atlantic and the global-scale warming trend. In addition, results show that regions with significant increases (decreases) in the mean value of precipitation relative to the control run also tend to see increases (decreases) in the frequency of pluvial (drought) events. Areas with increased frequency of extreme events also tend to show higher intensity extremes. There is general agreement between the five

Corresponding author address: Dr. Kirsten L. Findell, NOAA/GFDL, 201 Forrestal Road, Princeton, NJ 08540-6649.
E-mail: kirsten.findell@noaa.gov

DOI: 10.1175/2009JCLI3153.1

models on these impacts; differences between the model responses will also be discussed.

In the next section, we will discuss broad aspects of the five participating models. In section 3 we will define the drought measures used in this study. Results from the Pacific, Atlantic, and trend-based experiments will be discussed in section 4, prior to some discussion in section 5 and concluding statements in section 6.

2. Model descriptions and experimental design

The idealized SST experiments were performed with five different global atmospheric climate models:

1) the Geophysical Fluid Dynamics Laboratory (GFDL) used the Atmospheric Model, version 2.1 (AM2.1) (Delworth et al. 2006; The GFDL Global Atmospheric Model Development Team 2004; Milly and Shmakin 2002);
2) the Global Modeling Assimilation Office (GMAO) of the National Aeronautics and Space Administration (NASA) Goddard Space Flight Center (GSFC) used the NASA Seasonal-to-Interannual Prediction Project (NSIPP1) (Bacmeister et al. 2000);
3) the Community Climate System Model (CCSM) Climate Variability Working Group at the National Center for Atmospheric Research (NCAR) used the NCAR Community Atmosphere Model, version 3.5 (CAM3.5) (http://www.ccsm.ucar.edu/models/atm-cam/; Neale et al. 2008; Oleson et al. 2008; Stöckli et al. 2008);
4) the Climate Group of Lamont-Doherty Earth Observatory (LDEO) at the Columbia University used the NCAR CCM3 (Kiehl et al. 1998); and
5) the Climate Prediction Center (CPC) of the National Centers for Environmental Prediction (NCEP) used the NCEP Global Forecast System (GFS; Campana and Caplan 2005).

The five models will be referred to by the names GFDL, NSIPP, CAM3.5, CCM3, and GFS. Each of the models is documented in the references listed above and in Schubert et al. (2009, their Table 2), which provides an overview of the working group's initiative.

a. SST forcing fields

Figure 1a shows the SST climatology derived from the Hadley Centre data spanning the years 1901–2004 (HadISST; Rayner et al. 2003). A rotated empirical orthogonal function (EOF) analysis (Kaiser 1958) identified the three leading patterns of annual mean SST variability as a global trend pattern, a Pacific ENSO-like pattern, and an Atlantic pattern that resembles the Atlantic multidecadal oscillation (Kerr 2000; Enfield et al. 2001). These patterns represent 27.2%, 20.5%, and 5.8% of the global SST variance. Although the third EOF explains such a small percent of the global variance, it does explain up to 70% of the local variance in the region of the intertropical convergence zone (ITCZ) during northern summer. The analysis was restricted to ice-free points.

These patterns were scaled by the standard deviations of the respective principal component time series. The Pacific and Atlantic patterns were multiplied by twice the standard deviation of their respective principal components to create patterns similar to those observed in years of great extremes in these basins (Figs. 1c,d), while the linear warming trend was multiplied by one standard deviation to maintain a pattern with historical relevance (as opposed to a future warming pattern; Fig. 1b). The robustness of this trend pattern will be discussed in section 4e. These anomalies were then added to the climatological seasonal cycle of SST and used as the new boundary condition of the model's simulation.

b. Experimental design

Each modeling group ran a series of eight experiments with all possible combinations of a warm and cold Pacific and Atlantic forcing in addition to the control experiment (Table 1). When referring to these combination experiments, we will use the notation of Table 1: for example, PcAw refers to the experiment with both the cold Pacific and the warm Atlantic anomaly patterns added to the climatological SSTs of the control experiment; PwAn refers to the experiment with the warm Pacific and a neutral (or no) Atlantic pattern added to the climatology. All of the groups ran an additional experiment with the warm trend anomaly (Fig. 1b) added to the climatological SSTs. Four of the modeling groups ran the experiments for more than 50 years, while the GFS experiments were run for 37 years. The last 50 years are used when available; the last 36 years are used with the GFS results.

All of the experiments discussed in this paper are run with prescribed SSTs. Thus, while these experiments provide clear insight into the way SST anomalies can alter regional climate properties, they overlook the interesting question of further feedbacks and coupling to the SST fields. Such a study would require a full dynamic coupled model with an interactive ocean, beyond the scope of the present intercomparison project. Further discussion of the limitations of fixed-SST experiments is provided in section 5.

3. Drought and pluvial definitions

Drought can be defined in many ways, with many different spatial and temporal frames of reference. As

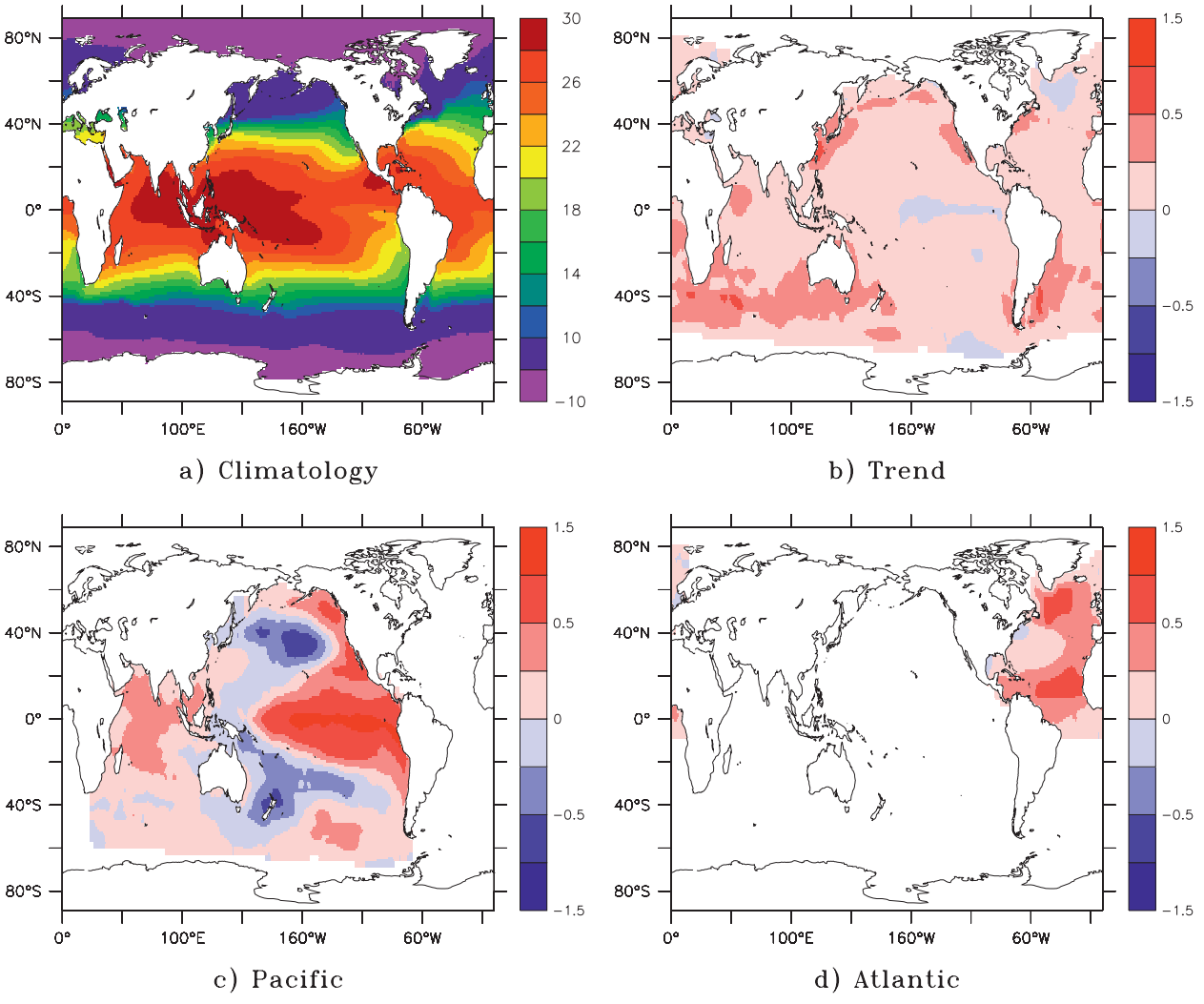

FIG. 1. SST forcing patterns: (a) climatology derived from the Hadley Centre dataset spanning the years 1901–2004; (b) warming trend anomaly; (c) Pacific warm-phase anomaly; and (d) Atlantic warm-phase anomaly.

a review of drought definitions by Wilhite and Glanz (1985) makes clear, there is not—and cannot be—one universal definition of drought, given the different time and space scales of interest in various meteorological, agricultural, and hydrologic resource issues. Precipitation (or lack thereof) is the primary factor in drought considerations, but temperature, radiation, the growth stage of vegetation, the ability of the vegetation to access groundwater, and many other factors play critical roles in the development or abatement of drought in the real world. The Drought Monitor (http://drought.unl.edu/dm) is a tool for tracking and displaying the magnitude and spatial extent of droughts within the United States, and it is founded on the assumption that no single index is suitable for all purposes or for all regions; maps are produced on a weekly basis after fusing objective data from a suite of drought-related indices and subjective data from on-the-ground experts in regions throughout the country (Svoboda et al. 2002).

We will rely on two indicators of drought and pluvial occurrence in this paper: 1) precipitation deciles as an indicator of meteorological drought, and 2) the supply–demand drought index (SDDI) as an indicator of longer-term drought. Both indices were justified in their original publications as improvements over the Palmer drought severity index (PDSI; Palmer 1965). The PDSI was a

TABLE 1. Suite of nine idealized experiments performed by each modeling group.

	Cold Pacific	Neutral Pacific	Warm Pacific
Cold Atlantic	PcAc	PnAc	PwAc
Neutral Atlantic	PcAn	PnAn (control)	PwAn
Warm Atlantic	PcAw	PnAw	PwAw

landmark development in drought research because it was the first water-budget-based index: it incorporated antecedent precipitation, moisture supply, and moisture demand into a hydrologic accounting system (Heim 2002). It was widely adapted to regions far from its original development zone in the Great Basin of the United States, despite Palmer's own warnings against such extrapolation (Heim 2002). Although no drought index has proven as popular as the PDSI, many studies have analyzed its weaknesses (e.g., Alley 1984), and others have developed improved versions (e.g., the self-calibrating PDSI of Wells et al. 2004; the modified PDSI of Mo and Chelliah 2006). Few recent studies claim that the PDSI is well suited to global analysis, and its continued usage in global studies is typically justified on the basis of its prevalence in past research (e.g., Shabbar and Skinner 2004).

Precipitation deciles were chosen as the meteorological measure of drought in the Australian drought watch system in 1992 (White and O'Meagher 1995). This index was more advantageous than others (particularly the PDSI) for a number of reasons including 1) the simplicity of the necessary data (precipitation would be needed for most drought indices; this required nothing else), 2) the lack of dependence on information regarding crop types and features, and 3) the applicability of deciles to any data distribution (not just normally distributed data) and the ease with which one can focus on extreme events (Gibbs and Maher 1967). The use of precipitation deciles is limited, however, by the failure to account for the impact of temperature or radiation as a driver of evapotranspiration and by the failure to account for the cumulative impact of prolonged spells of extreme precipitation (low or high values).

Deciles are sometimes used with additional criteria to determine when a drought is over (e.g., if the precipitation total for the past three months is in or above the eighth decile; Keyantash and Dracup 2002), though such criteria are not used in this study. Keyantash and Dracup (2002) gave rainfall deciles the highest evaluation score among six meteorological drought indices (PDSI among them) considered in their study of data from the state of Oregon. Here we will define drought in a given grid cell as months with precipitation below the 20% level of the control run (in the bottom two deciles or below the minimum observed value in the control run), and pluvials as months with precipitation above the 80% level of the control run (in or above the top two deciles).

Keyantash and Dracup (2002) considered five hydrological drought indices and five agricultural drought indices in their comparative study, but all of them are less than ideal for this model intercomparison because of their dependence on soil moisture and/or streamflow. Though soil moisture is clearly a critical factor in real-world droughts, modeled soil moisture is highly dependent on the land surface scheme of the given model and should not be taken as a volumetric measure of actual soil moisture. More importantly, soil moisture from different land surface schemes is reported for different depth levels and relative to different soil porosities and transmissivities. This makes it difficult to calculate soil moisture-dependent drought indices in a consistent manner when considering a suite of models. Streamflow reporting is similarly model dependent, making streamflow-dependent drought indices unsuitable for a model intercomparison.

The SDDI was first suggested by Rind et al. (1990) as an alternative to the PDSI. It is driven by the difference between the supply of moisture (precipitation P) and the atmospheric demand for moisture (potential evapotranspiration E_P). The SDDI has a few significant advantages over the PDSI. First, the index is tied to soil moisture through the evaporative demand, but it does not rely directly on the modeled value of soil moisture. Additionally, there are no grid-specific empirical coefficients to estimate. Its definition is similar in structure to that of the PDSI. First, a difference between the modeled value of $(P - E_P)$ and the monthly climatological value is calculated:

$$d = P - E_P - (P - E_P)_{\text{clim}},$$

where the climatology is determined from each model's control simulation. Then a "moisture anomaly index" is determined:

$$Z = \frac{d}{\sigma},$$

where σ is the interannual standard deviation in the monthly $(P - E_P)$ series from the control run climatology. Finally, the cumulative nature of drought is included in the final index for month i through the equation

$$\text{SDDI}(i) = 0.897\,\text{SDDI}(i-1) + Z(i).$$

The constant value of 0.897 was chosen by Rind et al. (1990) to mimic the PDSI. Threshold values of ± 2.0 are used as indicators of drought and pluvial. In the control run, this produces an average of 2.3 months yr^{-1} in each extreme. This is quite similar to the 20th and 80th percentile thresholds for precipitation deciles, which, by definition, produce 2.4 months yr^{-1} in drought or pluvial in the control run.

One of the beneficial qualities of the SDDI is the easy-to-understand notion of supply versus demand. However, the demand side of the equation has many potential definitions, and it depends on atmospheric conditions,

soil water availability, and vegetation type and growth stage. The concept of potential evaporation was first discussed in 1948 (Thornthwaite 1948) with the idea of defining some measure of atmospheric demand for moisture if soil moisture availability was not restricted and the vegetation covering over a large area was uniform. Numerical definitions stemming from this concept are plentiful, varied, and empirical. Some E_P definitions require only temperature information, while others require temperature and net radiation, and still others require these variables along with canopy conductance estimates for a specific vegetation type. Given the empirical nature of these equations, it is important to keep in mind that these relationships could change as climate changes. Thus, the E_P definition used here in SDDI calculations should be taken as an indicator of atmospheric moisture demand that may be sensitive to climatic conditions.

Our SDDI calculations make use of the radiation-based method of Priestley and Taylor (1972) for the calculation of E_P:

$$E_p = \frac{\alpha_{\mathrm{PT}}[s(T_a)]\,R_{\mathrm{net}}}{\rho_w \lambda_v [s(T_a) + \gamma]},$$

where $\alpha_{\mathrm{PT}} = 1.26$ was determined empirically from data over both water and saturated land surfaces, R_{net} is net radiation at the surface, T_a is air temperature, ρ_w is the mass density of water, λ_v is the latent heat of vaporization, γ is the psychrometric constant, and $s(T_a)$ is the slope of the relation between saturation vapor pressure (e_{sat}) and air temperature. Campbell and Norman (1998) show that a convenient, empirical equation for computing the saturation vapor pressure from temperature is the Tetens formula:

$$e_{\mathrm{sat}}(T) = a \exp\left(\frac{bT}{T + c}\right),$$

where the constants a, b, and c are chosen to optimize the fit for various ranges of data. This leads to

$$s(T) = \frac{de_{\mathrm{sat}}(T)}{dT} = \frac{bc}{(T + c)^2} e_{\mathrm{sat}}(T).$$

Campbell and Norman (1998) further state that, for environmental biophysics applications, appropriate values are $a = 6.11$ mb, $b = 17.502$, and $c = 240.97$°C; $s(T)$ appears in the E_p equation as $s(T)/[s(T) + \gamma]$. This ratio is not highly sensitive to the a-b-c estimates used, with two other empirical fits [Rogers and Yau (1989) suggest $a = 6.112$ mb, $b = 17.67$, and $c = 243.5$°C; Dingman (1994) suggests $a = 6.11$ mb, $b = 17.3$, and $c = 237.3$°C] yielding differences of that ratio of order 1×10^{-4}: three orders of magnitude smaller than $s(T)$ itself. Sensitivity studies varying $s(T)$ by two orders of magnitude showed that the SDDI is not highly sensitive to the details of the E_p calculation.

Though we believe that precipitation deciles and the SDDI are adequate indicators of large-scale changes in surface conditions, we are fully cognizant of the reality that no index is a perfect measure of drought or pluvials in all regions of the world.

4. Results

We begin our exploration of the results by taking an in-depth look at the cold Pacific experiment (PcAn) with the GFDL model as a way of detailing the methodologies used in this work. We will then look at results of the PcAn and the PnAw experiment with all five models as well as the multimodel mean to show some of the differences between the models. Subsequent results will only include plots of the multimodel mean (MMM).

a. Cold Pacific experiment

Figure 2 shows some results of the cold Pacific experiment with the GFDL model. Mean precipitation differences (Fig. 2a) highlight the same regions of change as indicated by mean SDDI differences (Fig. 2b). Results are shown over land only since the SDDI is a quantity with little relevance to the ocean where the ''supply'' part of the index is always unlimited. In both plots, differences are shaded only where they are statistically significant at the 95% level according to the modified t test of Von Storch and Zwiers (1999; the test is modified to account for autocorrelation within the time series; see Findell et al. 2006). Additionally, both plots show a large percentage of land area passing the t test: 30.9% passes the 95% level test in Fig. 2a and 33.2% in Fig. 2b. This is far greater than the 5% expected to pass by chance, and the 10%–15% that would be required by a field significance test accounting for reduced degrees of freedom caused by spatial dependence between neighboring grid cells (see, e.g., Findell et al. 2006). Both plots show regions of decreases in the mean values in the central United States and southern South America, and to a lesser extent in Alaska, central Africa, and central Asia. Regions of increases in the means occur in southern Central America and north- and central-eastern South America (including Amazonia) and to a lesser extent in Indonesia, Australia, the Arabian Peninsula, and southern Africa. The similarity between Figs. 2a and 2b is a reflection of the SDDI being driven primarily by precipitation. The differences between these plots indicate that SDDI is generally a more sensitive index than precipitation deciles. This is likely a

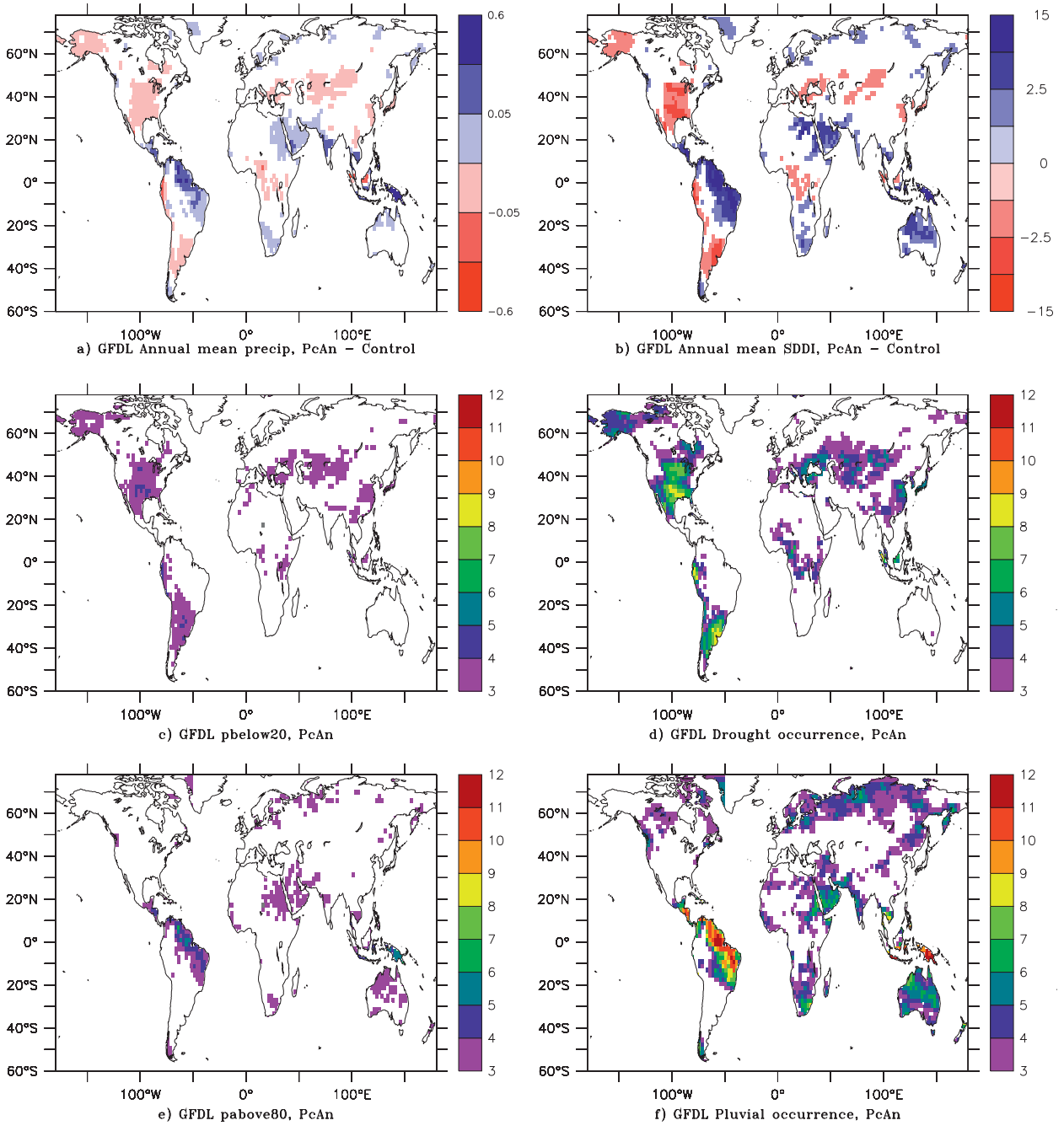

FIG. 2. Results of the cold Pacific experiment (PcAn) with the GFDL model: (a) mean precipitation differences from control run (cm day^{-1}), shaded where significant at the 95% level; (b) mean SDDI differences from the control run, also shaded where significant at the 95% level; (c) average number of months yr^{-1} with precipitation below the 20th percentile of the control run; (d) average number of months yr^{-1} with SDDI below −2.0; (e) average number of months yr^{-1} with precipitation above the 80th percentile of the control run; (f) average number of months yr^{-1} with SDDI above 2.0.

result of the two primary differences between the two indices: the SDDI is dependent on temperature and radiation, in addition to precipitation, and the SDDI has some accounting for the cumulative nature of drought.

The second row of Fig. 2 highlights regions with increased drought occurrence as measured by the average number of months yr^{-1} with precipitation below the 20th percentile level of the control run (Fig. 2c) and by the average number of months yr^{-1} with SDDI below

−2.0 (Fig. 2d). By definition, each grid cell in the control run has 2.4 months yr^{-1} below the 20th percentile precipitation threshold. The SDDI value of −2.0 marks a similar threshold: grids cells in the control run have values below this threshold on average 2.3 months yr^{-1}. Grid cells with fewer than 3.0 months yr^{-1} below the respective thresholds are not shaded in Fig. 2c or 2d. This shading threshold was chosen as a surrogate for significance. We know that a binomial distribution of 600 sample members (50 years, 12 months each), each with a probability of success of 0.2 (20% of the sample in the 20th percentile), would exceed the 95% significance threshold if 136 or more sample members (or 2.72 months yr^{-1}) were categorized as successes. The likelihood of 150 or more sample members (or 3 months yr^{-1}) being successes is only 0.12%. Clearly the individual months in these sample datasets are not independent, so they do not satisfy the requirements of a binomial probability distribution. Nevertheless, the likelihood of 3 or more months yr^{-1} falling into the 20th percentile if the probability distribution is unchanged from the control run is very small. Further significance testing was not performed, in part because the regions of increased drought frequency shaded in Figs. 2c,d are largely coincident with regions of decreases in the mean precipitation and the mean SDDI (Figs. 2a,b), which have been shown to be statistically significant.

These measures of drought occurrence—monthly precipitation or SDDI compared to a climatological norm—do not account for the fact that some months are more important than others in drought considerations. In many cases, a relative dry spell during an already dry month can be ameliorated by normal rainfall during the rainiest time of the year, while rainfall deficits during the rainy season are much more difficult to make up. However, given the global nature of this analysis, we felt it was important to include all months of the year. For a more detailed analysis of individual regions, a seasonal approach might be warranted.

The bottom row of Fig. 2 provides similar information about the occurrence of pluvials in this cold Pacific experiment. Figure 2e shows slight increases in the average number of months yr^{-1} with precipitation exceeding the 80th percentile of the control run. These areas are largely coincident with regions with increased mean precipitation (Fig. 2a). Figure 2f shows locations with increased occurrence of SDDI values greater than 2.0. These areas are largely coincident with areas of increases in mean SDDI (Fig. 2b).

Though the locations of increased drought and pluvial occurrence are generally consistent between the precipitation deciles (Figs. 2c,e) and the SDDI calculations (Figs. 2d,f), the average number of months yr^{-1} in an extreme is much higher in the SDDI plots than in the precipitation decile plots. As discussed above in regard to the mean precipitation and SDDI differences, these differences in drought and pluvial occurrence stem from the additional climatic information included in the SDDI calculation and from the short-term (individual months) perspective of deciles, versus the cumulative nature of the SDDI. This relationship between the two measures of drought is seen in all experiments and with all models. Consequently, we will only show SDDI values in subsequent plots.

Figures 3 and 4 show the SDDI-based drought and pluvial frequency for the cold Pacific experiment for each of the five participating models, as well as for the MMM. The results of the MMM shown in Figs. 3f and 4f closely match the results from the GFDL model discussed above in regard to Fig. 2 and shown again in Figs. 3a and 4a. These impacts include increased drought frequency in the continental United States and southern South America and to a lesser extent in southern Europe into central Asia and along the southeastern coast of Asia. Additionally, we see increased pluvial frequency in southern Central America, northern and central South America, and to a lesser extent Australia, Arabia, India, and southern Africa. All of the models show these same general results, with notable variations in the spatial extent of the responses and the intensity of the increases, particularly in Africa and Europe. Most notably, the CAM model shows greater increased pluvial frequency throughout northern Africa than the other models. In general, peak values of drought and pluvial frequency for a given region are highest in the CAM results and lowest in the GFS results.

Figures 5 and 6 show a measure of drought and pluvial intensity for the cold Pacific experiment for each of the five models and the MMM: the average value of the SDDI when the SDDI exceeds the −2.0 and +2.0 thresholds. For all the models in general, and particularly in the MMM, the regions of increased drought occurrence (Fig. 3) tend to coincide with regions of increased drought intensity (Fig. 5). Similarly, Figs. 4 and 6 show that the highest SDDI intensities occur where high SDDI values occur more frequently. Additionally, comparison of Figs. 5 and 6 shows that high-end extremes tend to be larger in magnitude than low-end extremes. This is likely a reflection of the long tail on the high end and the zero limit on the low end of precipitation distributions.

b. Warm Atlantic experiment

Figure 7 shows that all five models indicate increased drought activity in the continental United States in

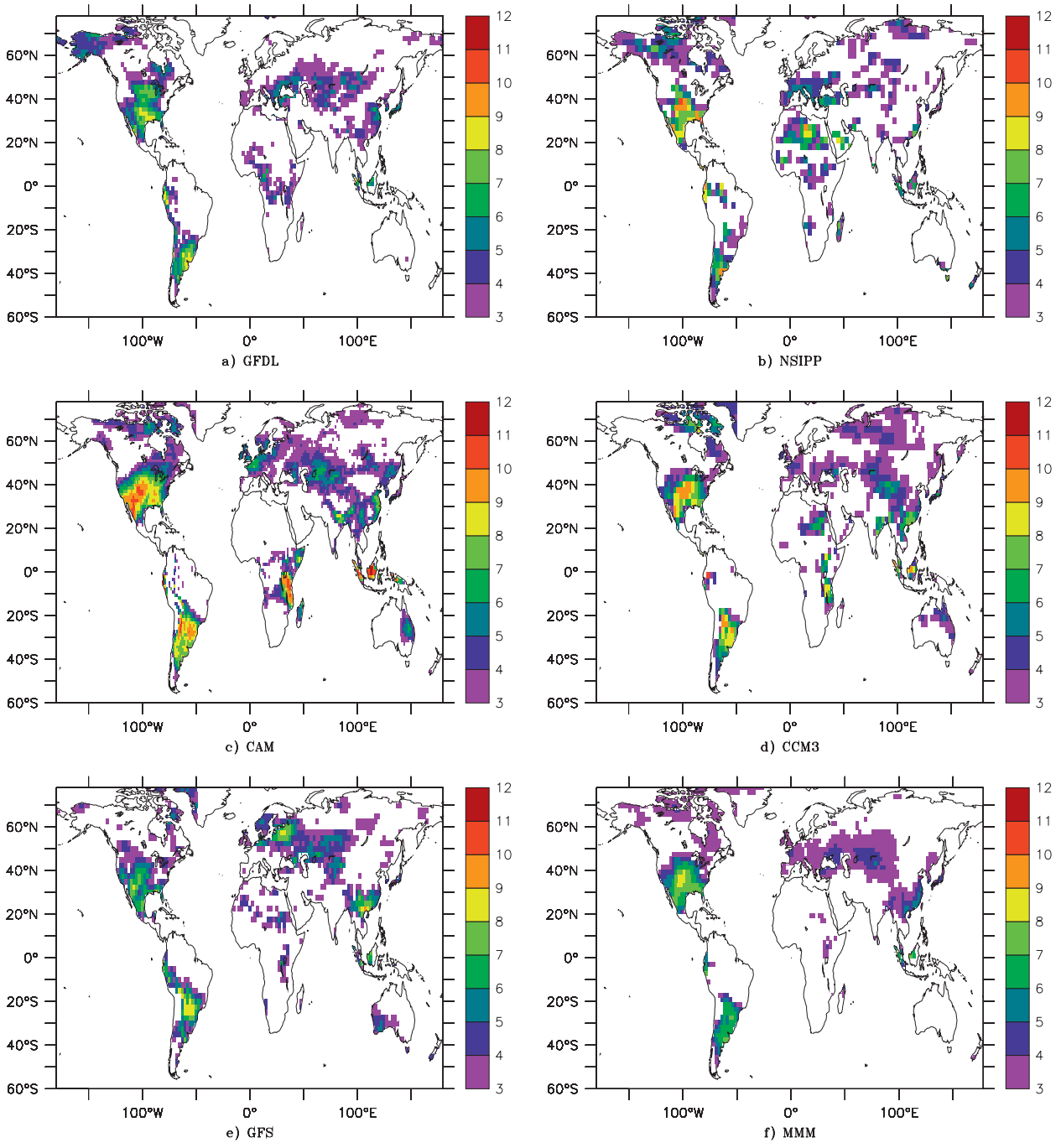

FIG. 3. Average number of months yr^{-1} in drought (SDDI < -2.0), relative to each model's control run, for the cold Pacific experiment: (a) GFDL, (b) NSIPP, (c) CAM, (d) CCM3, (e) GFS, and (f) MMM.

response to the warm Atlantic experiment (PnAw), though details of the responses certainly differ. The MMM shows a broad region with increased drought frequency, though the peak is only 4 months yr^{-1} in drought, as opposed to 8 months yr^{-1} in response to the PcAn forcing. Other regions showing increased drought frequency include central South America and modest increases in southern Europe, Alaska, southern Australia, and scattered sections of Southeast Asia. CCM3 shows a very strong response in Africa, extending into the Middle East and much of Asia, but these increases are not borne out in the MMM.

Four of the five models show a very strong increase in pluvial activity in southern Central America and

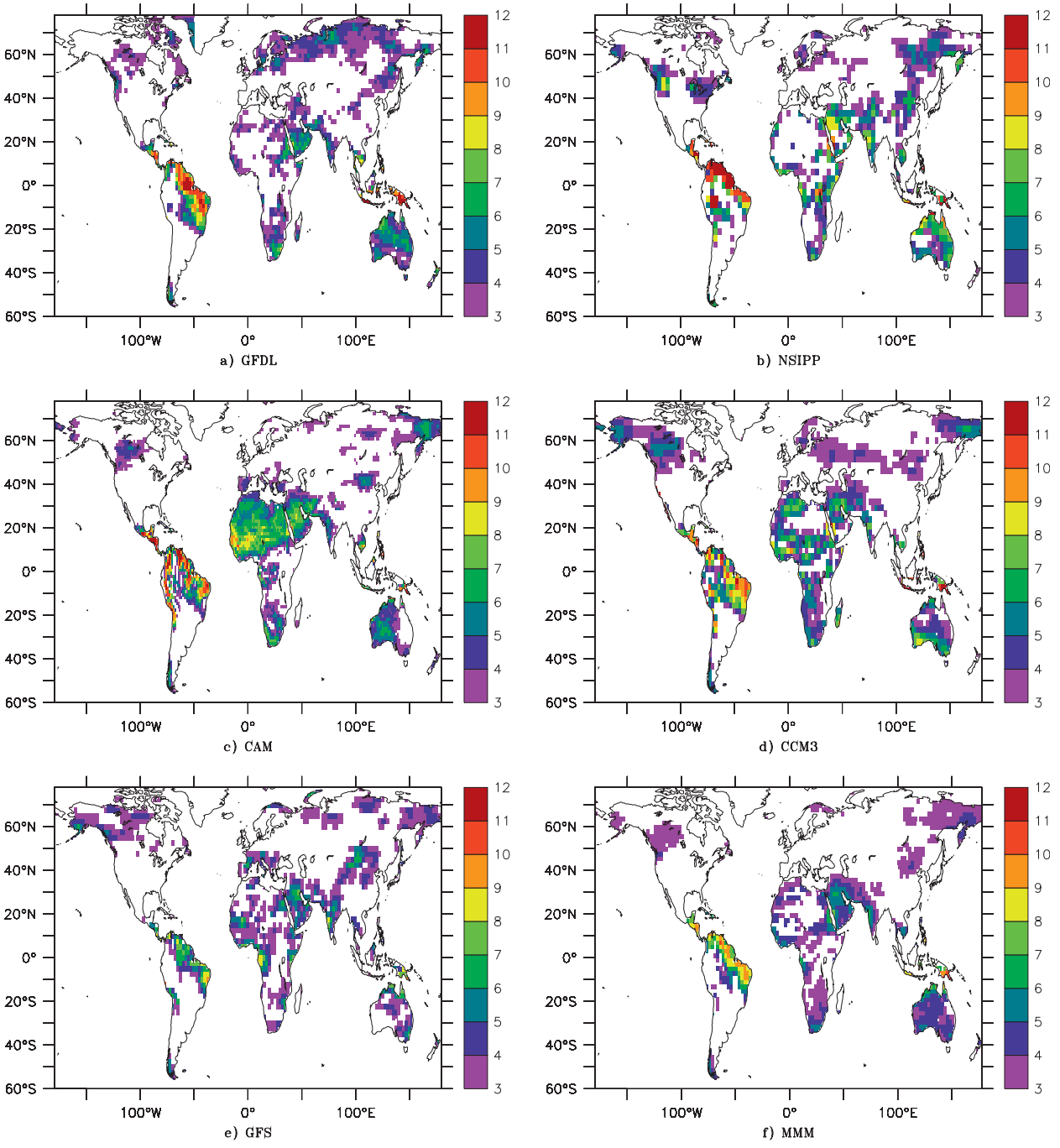

FIG. 4. As in Fig. 3, but for pluvial occurrence (SDDI > 2.0) with the cold Pacific experiment.

northernmost South America, extending across the Atlantic and into the Guinea Coast of Africa in response to PnAw (Fig. 8). GFS shows a much more modest response to this anomaly than the other models. CAM's response is the most intense in number of months yr^{-1} in pluvial, and the extent of the response is much broader in Africa than the other models show. The MMM also shows a modest increase in pluvial across much of northern Europe and Asia and in Indonesia.

c. *Warm Pacific experiment*

Figures 9 and 10 show MMM SDDI-based drought and pluvial frequencies for each of nine experiments shown in Table 1. The central figures indicate that only

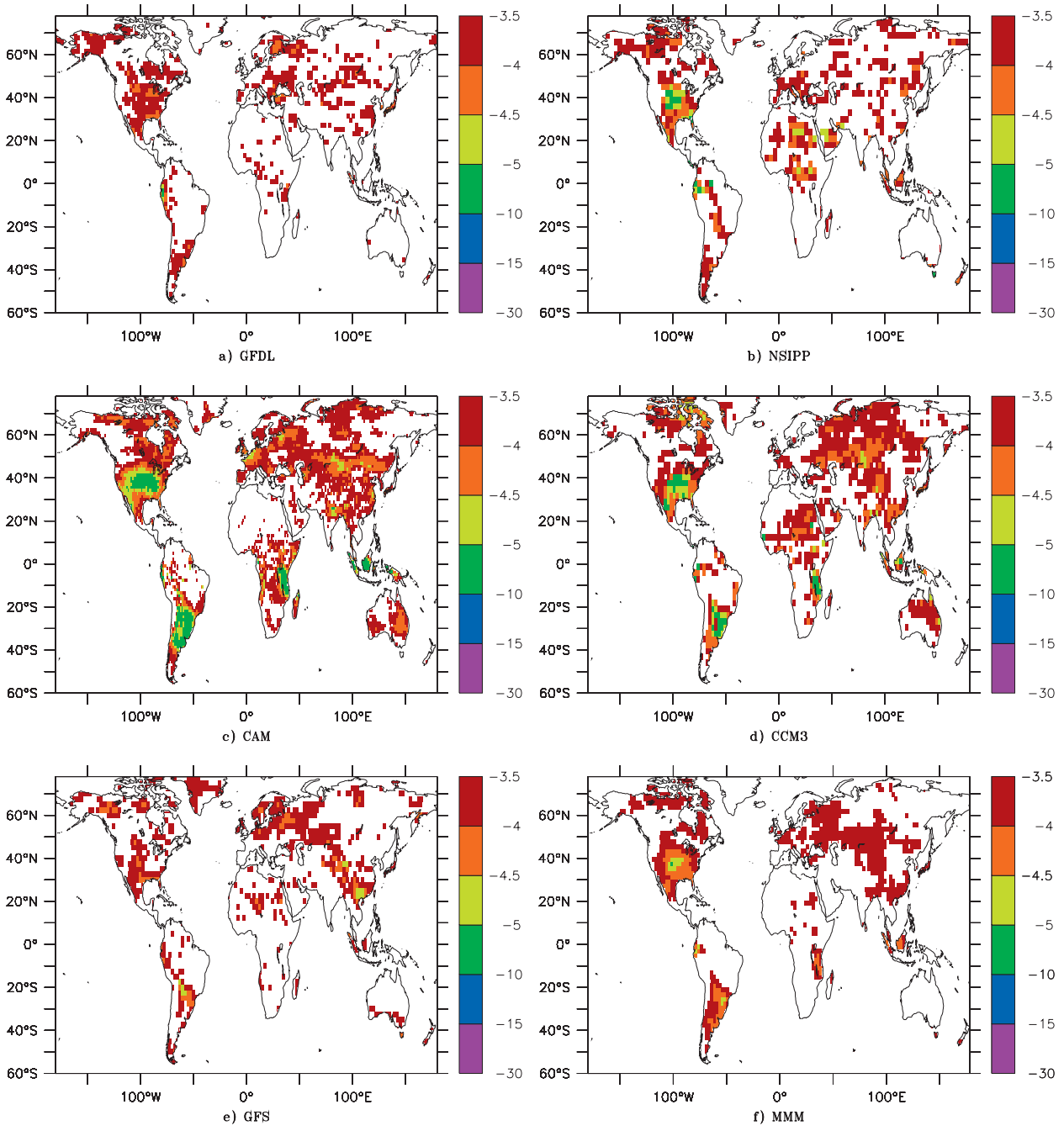

FIG. 5. Drought intensity in the cold Pacific experiment, as measured by the mean SDDI value during times of drought (when SDDI < -2.0).

a handful of grid points in the control run have SDDI values lower than -2.0 or higher than 2.0 for more than 3 months yr^{-1}. Figures 9d and 10d are the same as Figs. 3f and 4f, respectively, showing drought and pluvial frequency for the cold Pacific experiment. Figures 9f and 10f show that the warm Pacific experiment generally leads to a reversal of the cold Pacific pattern: where the cold Pacific increases drought, the warm Pacific increases pluvials and vice versa. In both cases, the number of months yr^{-1} tend to be slightly higher on the pluvial side: for example, Fig. 10f shows peak values of over 9 months yr^{-1} in the central United States in pluvial with the warm Pacific forcing, while the cold Pacific forcing results in peak values of 8 months yr^{-1} in the same location (Fig. 9d). There are additional differences in the spatial signatures in areas with less pronounced increases. The cold Pacific experiment showed modest drought increases in southern Europe extending

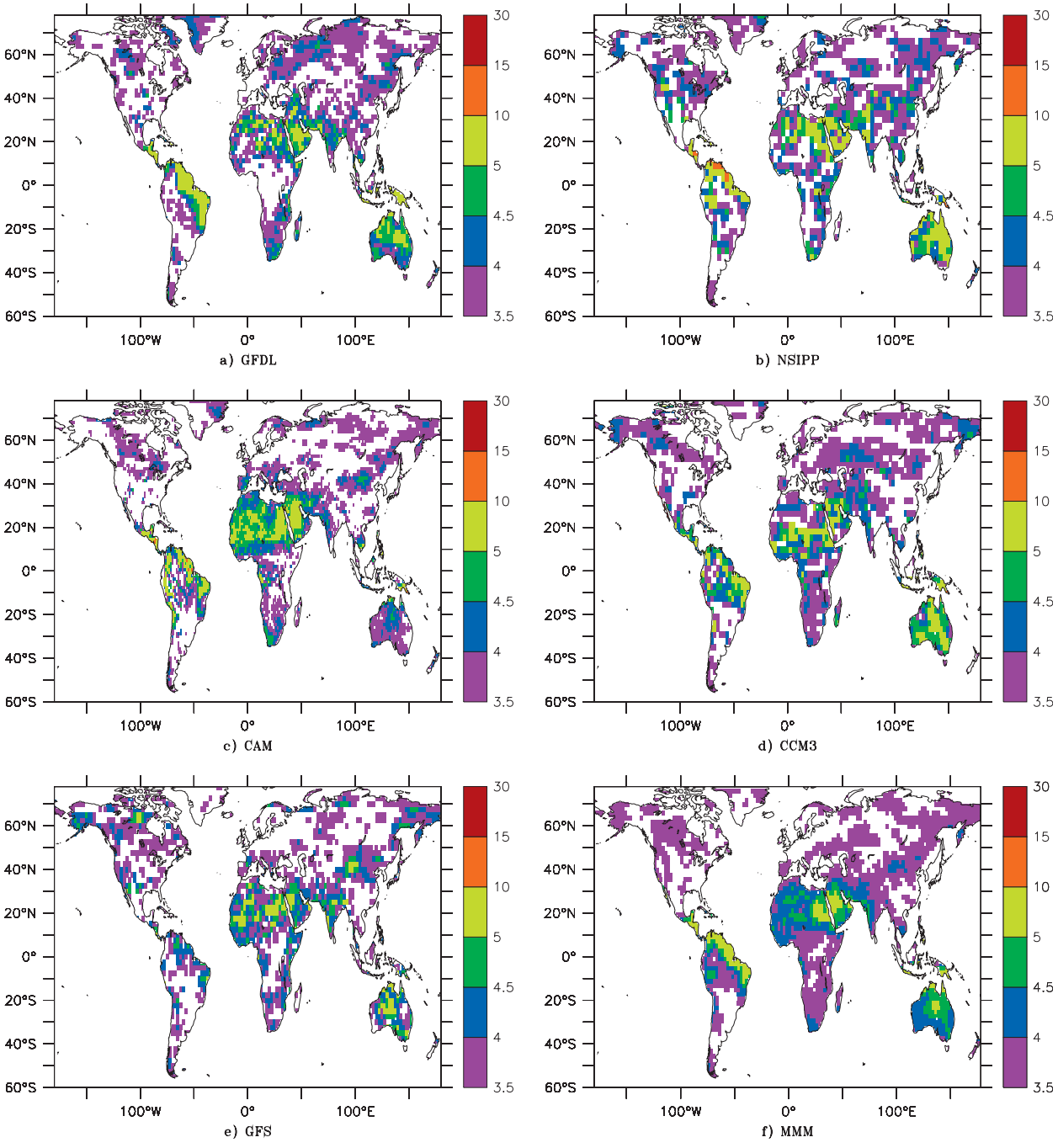

FIG. 6. Pluvial intensity in the cold Pacific experiment, as measured by the mean SDDI value during pluvials (when SDDI > 2.0).

into central Asia, for example. The warm Pacific experiment shows pluvial increases over a much broader portion of Europe but few grid points with values above 3 months yr^{-1} in central Asia. There are additional differences around the Indian Ocean: the cold Pacific experiment leads to increased pluvial in the Arabian Peninsula and India, while the warm Pacific experiment leads to increased droughts along the east coast of Africa. Nevertheless, to first order, the warm Pacific and the cold Pacific anomalies lead to opposite drought and pluvial impacts in most regions of the world.

d. Cold Atlantic experiments

The warm and cold Atlantic forcings also lead to generally opposite results. Figures 9b and 10b show the

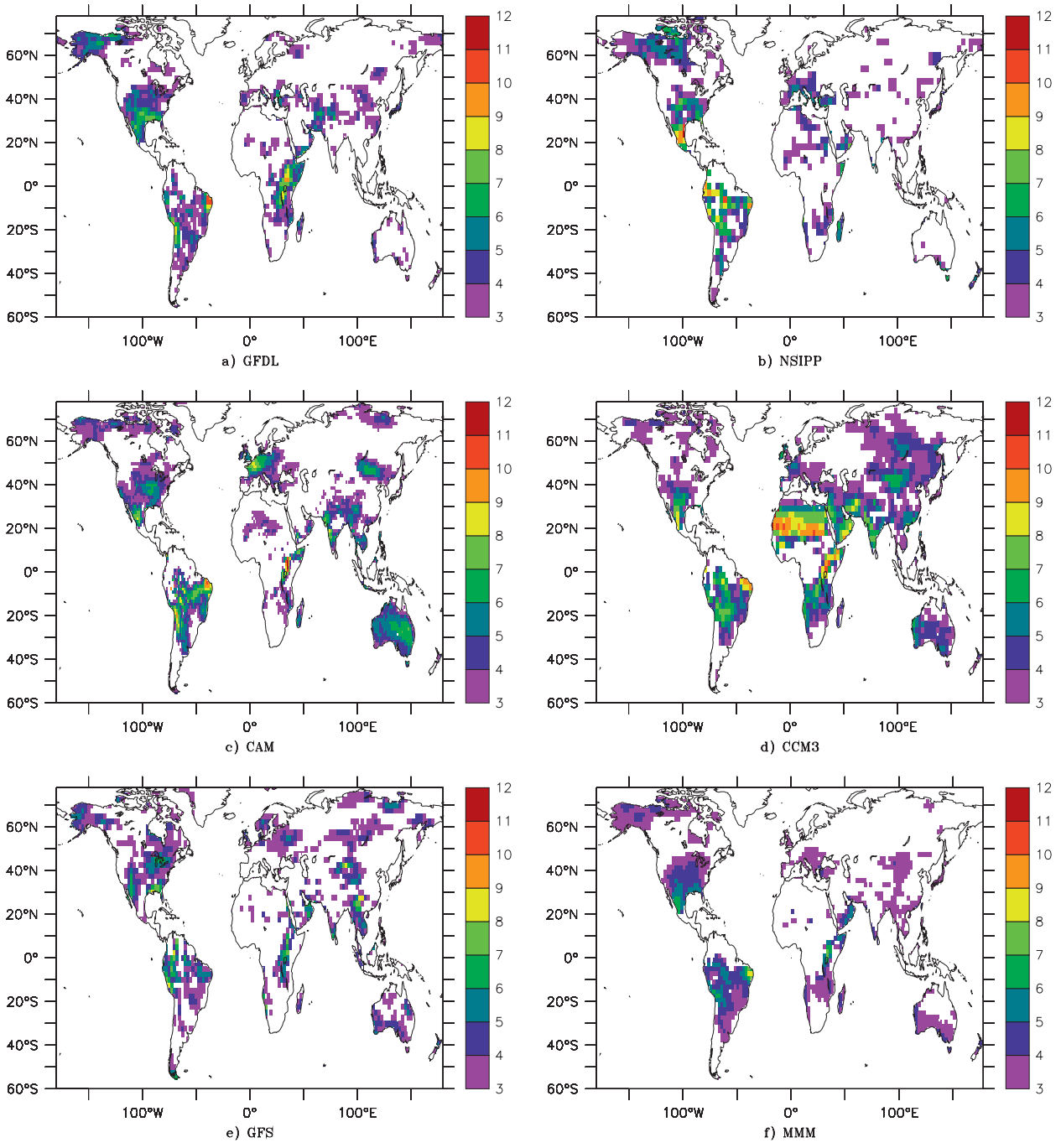

FIG. 7. Drought occurrence in the warm Atlantic experiment, as in Fig. 3.

drought and pluvial frequency with the cold Atlantic forcing, and Figs. 9h and 10h show the same plots for the warm Atlantic forcing (identical to Figs. 7f and 8f). The cold Atlantic forcing leads to increases in drought occurrence in southern Central America, northern South America, and a narrow region along the Guinea Coast of West Africa and into the Congo region. Increases in pluvials are seen in central South America, extending south into northern Argentina. Modest pluvial increases are seen in the continental United States and northern Mexico. Modest drought increases are seen in much of northernmost Asia. This is largely a reversal of the patterns discussed in section 4b in regard to the warm Atlantic experiment.

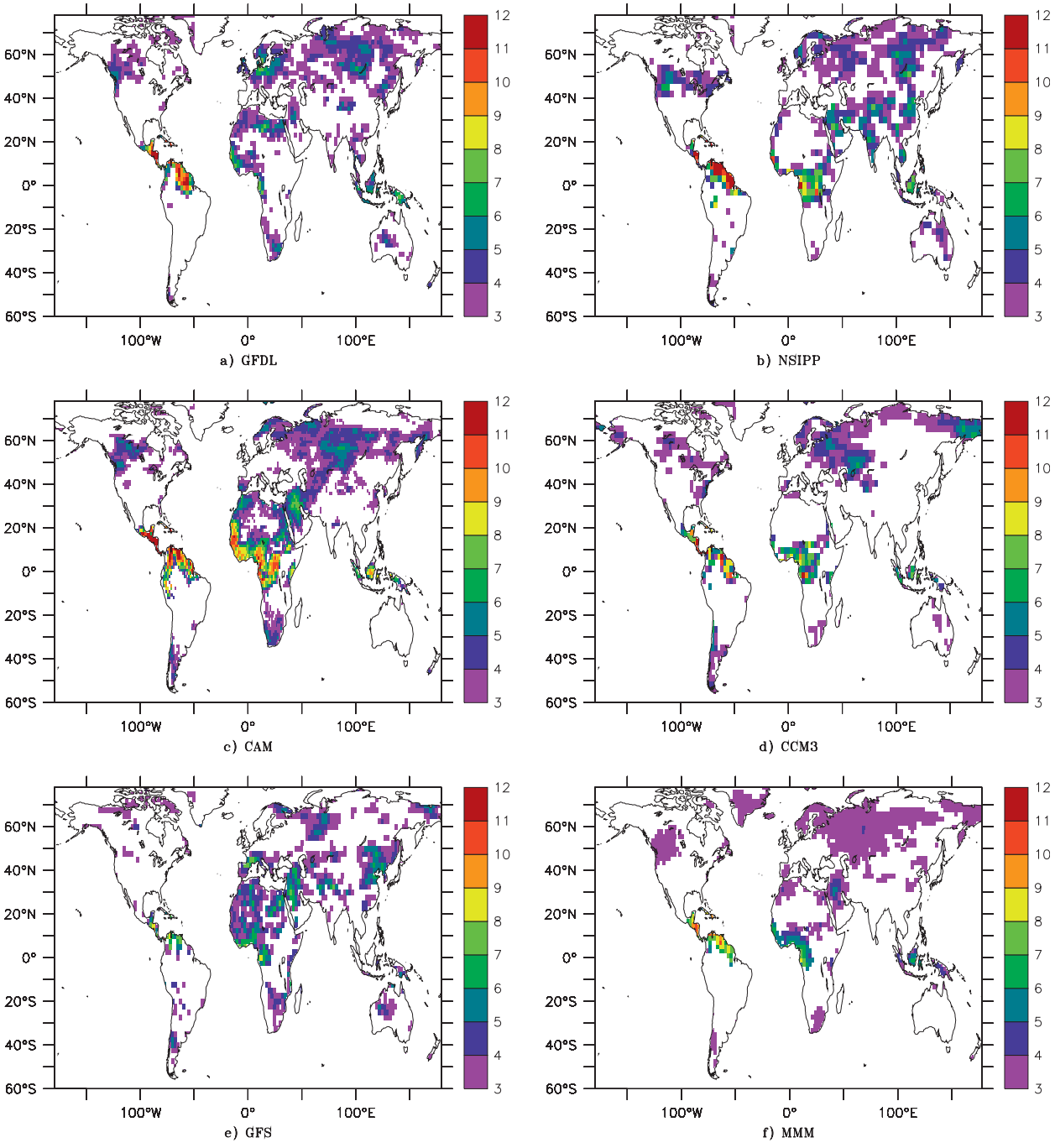

FIG. 8. As in Figs. 3, 4, and 7, but for pluvial occurrence in the warm Atlantic experiment.

e. Pacific–Atlantic combination experiments

Drought occurrence results for the four combination experiments (PcAc, PwAc, PcAw, and PwAw) are shown in the four corner subplots of Fig. 9. To first order, the results of the combination experiments most closely resemble their Pacific counterpart with a neutral Atlantic, indicating that, for most parts of the globe, the Pacific forcing is more dominant than the Atlantic. This is not entirely surprising, given the much broader spatial footprint and maximum intensity of the Pacific pattern (Fig. 1c) compared to the Atlantic pattern (Fig. 1d). Nevertheless, the Atlantic impacts are still substantial. In fact, Atlantic and Pacific impacts along the Guinea

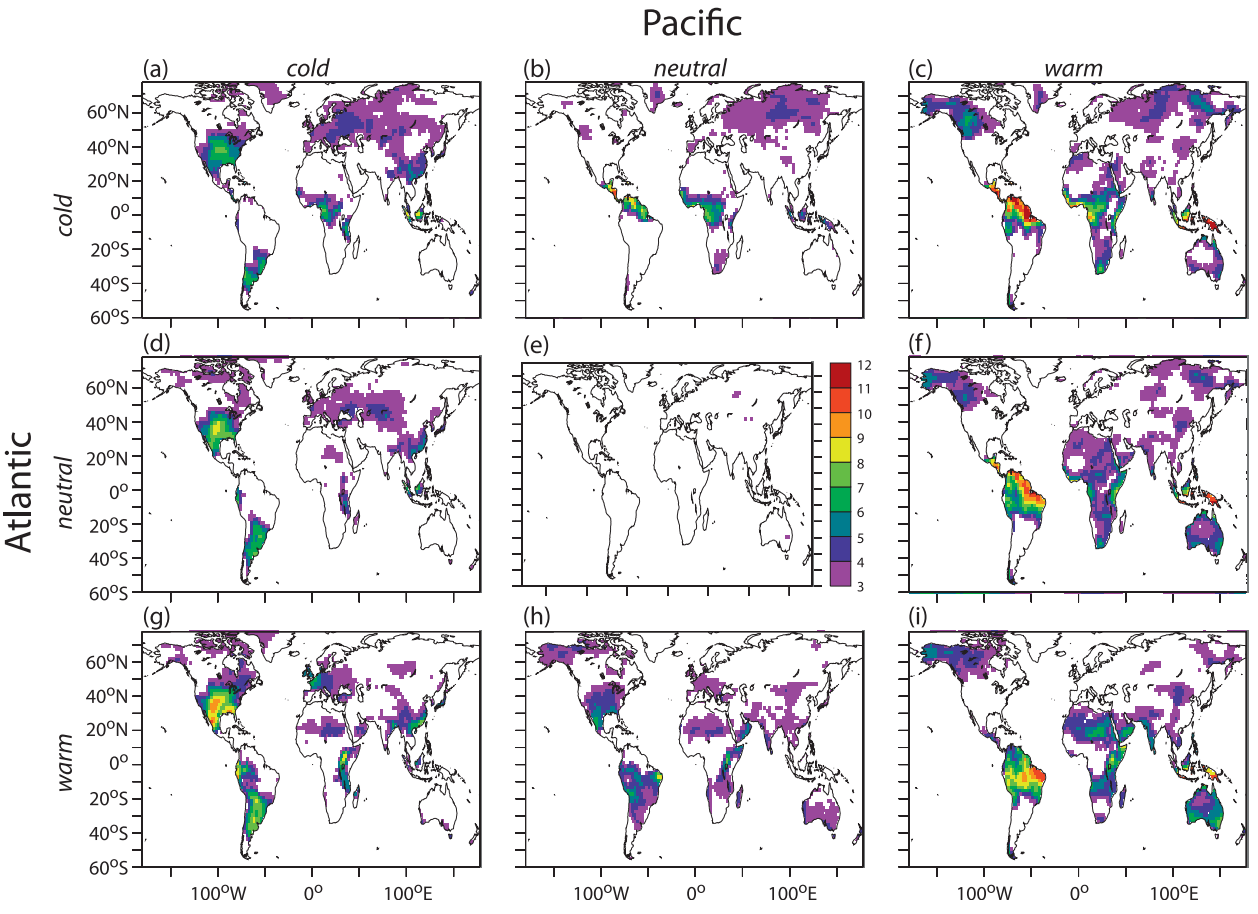

FIG. 9. Multimodel mean drought occurrence (average number of months yr^{-1} with SDDI < -2.0) for nine experiments: (a) PcAc, (b) PnAc, (c) PwAc, (d) PcAn, (e) PnAn (control), (f) PwAn, (g) PcAw, (h) PnAw, and (i) PwAw.

Coast and in the Congo region of Africa seem about equal in strength, with drought frequency maximized in the warm Pacific–cold Atlantic (PwAc) experiment (Fig. 9c). Though pluvial frequencies are maximized in the cold Pacific–warm Atlantic (PcAw) experiment (Fig. 10g), all of the experiments with a warm Atlantic increase pluvial frequency in these regions, with the broadest area of response occurring in the warm Pacific–warm Atlantic (PwAw) experiment (Fig. 10i).

For much of North and South America, the Atlantic and Pacific patterns work in opposition to each other: drought occurrences are maximized in North America and southern South America in PcAw. Pluvial occurrences in these regions are maximized in PwAc. For southern Central America and northern South America, drought occurrences are maximized in PwAc, and pluvial occurrences are maximized in PcAw. The Amazonian region is the exception: here the two forcings work in parallel, with drought occurrences maximized in PwAw and pluvial occurrences maximized in PcAc.

Impacts in Australia and the islands to the north are largely determined by the Pacific forcing, with all warm Pacific experiments leading to increased drought frequency and all cold Pacific experiments leading to increased pluvial frequency. The warm Atlantic anomaly increases the frequency of drought in Australia, whereas the cold Atlantic anomaly increases the frequency of pluvials.

Impacts are modest in Europe and Asia, with MMM values of months yr^{-1} in an extreme rarely surpassing 4. This modest impact is seen over the largest area with droughts in PcAc and with pluvials in PwAw.

f. Trend experiments

Figure 11 shows the MMM results of the experiment with the warm linear trend pattern shown in Fig. 1b added to the climatology shown in Fig. 1a. Both the drought plot (Fig. 11a) and the pluvial plot (Fig. 11b) show that the impact of the warm trend experiment is generally much smaller than the impact of the other two anomaly patterns.

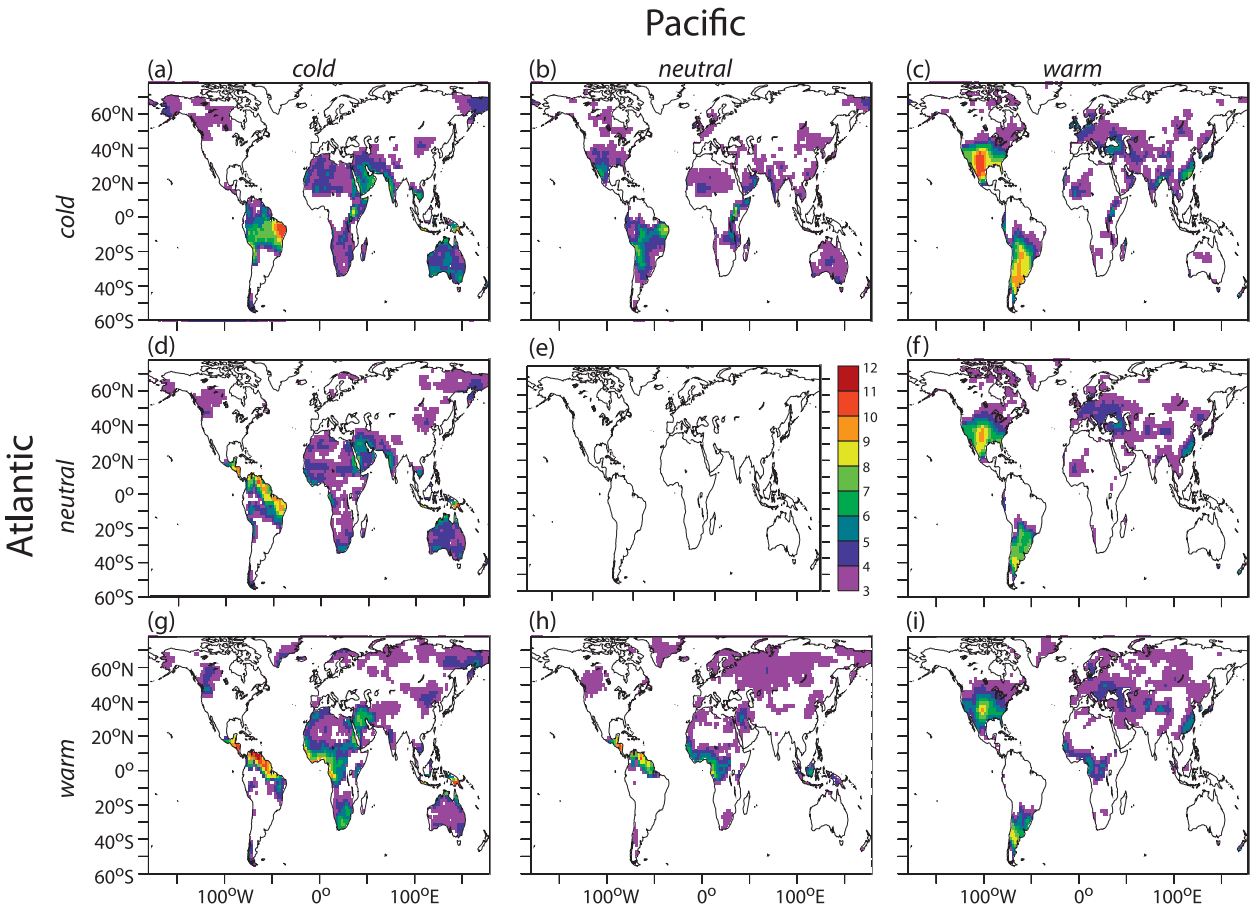

FIG. 10. As in Fig. 9, but for pluvial occurrence.

5. Discussion

It is worth noting that the SST forcing patterns used in this study were not derived in order to maximize drought or pluvial impacts in any particular location. On the contrary, the forcing patterns were determined from an unbiased EOF analysis aimed at isolating the leading patterns of variability in the global oceans. The results presented in this paper are largely in agreement with previous studies on the impact of Pacific and Atlantic forcing of precipitation and of drought in various regions of the world. Hoerling and Kumar (2003), Schubert et al. (2004), Seager et al. (2005), Herweijer and Seager (2008), and many others provide compelling evidence for the strong global-scale forcing from the tropical Pacific. Each of these studies shows that drought in much of the United States in particular and throughout the midlatitudes in general tends to occur when the eastern tropical Pacific is cooler than normal (La Niña conditions). Seager et al. (2003) explain that this impact is driven by changes in the locations of the subtropical jets and the effects these jets have on the eddy-driven mean meridional circulation. Hoerling and Kumar (2003), Schubert et al. (2004), and others extend this result to show that a warm Atlantic further exacerbates midlatitude drought conditions. Though the anomaly patterns they discuss are different from the ones used in this study, particularly in the western Pacific, our results with the PcAw experiment largely confirm their conclusion that cold Pacific and warm Atlantic conditions are well suited to midlatitude drought.

Some results do indicate that not all midlatitude regions are most prone to drought when the Pacific is anomalously cold and the Atlantic anomalously warm. Shabbar and Skinner (2004), for example, find a six-month lag relationship between winter warm Pacific conditions and summer drought conditions in western Canada. The warm Pacific combination experiments presented here show modest increases in drought frequency in western Canada (Figs. 9c,f,i), with the impacted region extending farthest south in the PwAc experiment.

McCabe et al. (2004) find an association between multidecadal variations in Atlantic SSTs and precipitation

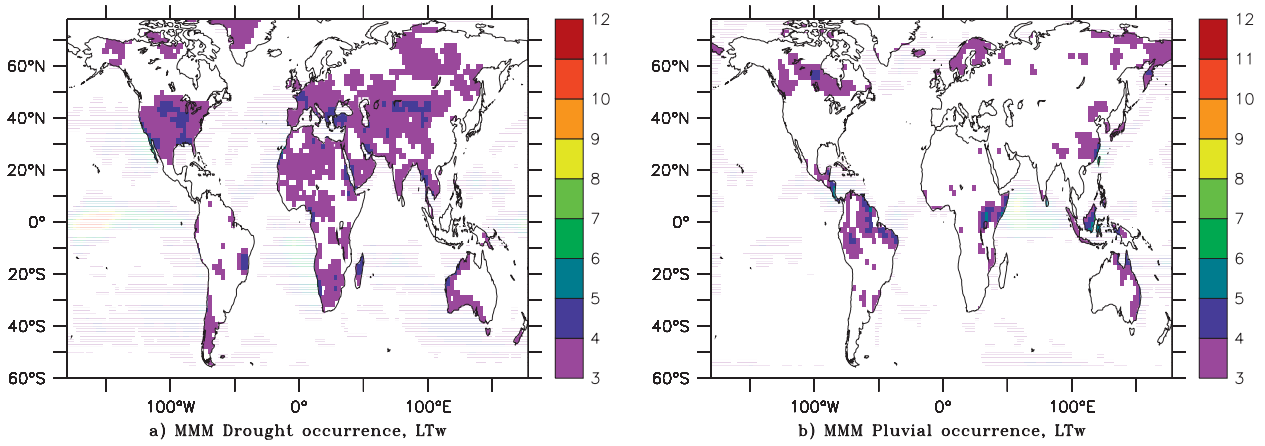

FIG. 11. (a) Drought and (b) pluvial occurrence in the warm trend experiment for the MMM.

and surface temperature changes in the United States, and Sutton and Hodson (2005) report similar findings for both Europe and the United States. Warm Atlantic SSTs were found to lead to temperature increases in both regions (with larger magnitudes and larger regions of significance in the United States), precipitation reductions in the United States, and precipitation increases in Europe. Thus, impacts of Atlantic SST variations on drought inferred from their findings would be more substantial in the United States than in Europe. This is consistent with findings presented here.

Much research has focused on the region encompassing southern Central America, the Caribbean Sea, and northeastern Brazil. In the results presented here, the Pacific influence in the Caribbean and northern South America is of uniform sign over a region extending south to about 18°–20°S latitude (warm Pacific increases drought occurrence, Fig. 9f; cold Pacific increases pluvial occurrence, Fig. 10d). The Atlantic influence in this region extends southward to about 5°S latitude (warm Atlantic increases pluvials, Fig. 10h; cold Atlantic increases droughts, Fig. 9b). North of 5°S, SST anomalies of opposing signs are associated with the greatest propensity to drought or pluvial: a cold Pacific and a warm Atlantic are most conducive to pluvials (Fig. 10g), while a warm Pacific and a cold Atlantic are most conducive to droughts (Fig. 9c). From about 5° to 20°S, anomalies of the same sign are associated with the greatest propensity to drought or pluvial: cold SSTs in both basins yield the most pluvials (Fig. 10a), and warm SSTs in both basins yield the most droughts (Fig. 9i). These results are confirmed by a wide range of studies (e.g., Hastenrath 1978; Enfield and Alfaro 1999; Giannini et al. 2001).

Studies about rainfall in the Sahel and the Guinea Coast of Africa indicate the importance of SST conditions adjacent to the region (Giannini et al. 2003). This is consistent with our finding that the Atlantic impacts more strongly on this region than the Pacific. However, other research indicates that the cross-equatorial SST gradient in the Atlantic is critical to precipitation conditions in this region (Fontaine and Janicot 1996; Hoerling et al. 2006), while still other research highlights the importance of uniform warming to drying in the Sahel (particularly with the GFDL Climate Model version 2.0 (CM2.0; Held et al. 2005). Drought occurrence in the runs reported here does increase in the Sahel in the warm trend experiment in the GFDL model, with a range of 3–6 months yr^{-1} in drought in the Sahel (not shown). The MMM, however, shows that much of the region has less than 3 months yr^{-1} of drought (Fig. 11a). The Hoerling et al. (2006) paper also shows a connection between Indian Ocean warming and drying in southern Africa. Both the warm trend and the warm Pacific forcings include warming in the Indian Ocean (Figs. 1b,c), and results of these experiments do indeed show moderately increased drought frequency in southern Africa (Figs. 9f and 11a).

Fundamental research on the ENSO phenomenon indicates that rainfall in Indonesia and the surrounding areas broadly termed Oceania is strongly linked to SSTs in the tropical Pacific, with warm conditions in the eastern tropical Pacific yielding more rain than normal in that area and far less rain than normal in Oceania (e.g., Hendon 2003). This is consistent with the picture of increased drought in Indonesia in our MMM results in each of the warm Pacific experiments, almost independent of the Atlantic condition (Figs. 9c,f,i), and increased pluvials in Indonesia in each of the cold Pacific experiments (Figs. 10a,d,g).

Xin et al. (2006) find a connection between winter North Atlantic Oscillation (NAO) and late spring cooling in the upper troposphere over central China. This

upper-troposphere cooling is associated with late spring drought in south China in the decades after about 1980 when the winter NAO shifted to a positive phase. The PnAw experiment yields a very modest increase in drought frequency over southern China (Fig. 9h), but further validation of the Xin et al. (2006) results would require additional analysis of other fields.

Research on the connections between Australian rainfall and ENSO events in the Pacific indicate a high degree of temporal variability in the relationship (Cai et al. 2001; Suppiah 2004). Indeed, Cai et al. (2001) show that, though there is typically a strong association between drought in northeastern Australia and warm conditions in the eastern tropical Pacific, this relationship has reversed on a number of occasions, most notably during the period 1931–45. They note that this weakening in the ENSO–rainfall relationship occurs when the linearly detrended global mean temperature is particularly high, though they do not determine a cause for the weakening. Rainfall in southwest Western Australia has been shown to be dependent on interactions between Indian Ocean SSTs and wind fields (England et al. 2006). However, other research indicates that fixed-SST experiments are of limited use in areas where rainfall has a strong impact on the temperature of the underlying ocean (e.g., Lau and Nath 2000; Wang et al. 2005; Bracco et al. 2007). Wang et al. (2005) show that the feedbacks between the atmosphere and the Indian ocean cannot be neglected in simulation of the Asian–Pacific summer monsoon rainfall, and Bracco et al. (2007) try to determine which areas of the tropical oceans must interact with the atmosphere to properly capture the relationship between ENSO and the Asian summer monsoon. Numerous studies have also pointed out that some of the limitations in simulating monsoon rainfall, particularly in this region, may be due to model biases in capturing the mean state (see, e.g., Zhou et al. 2008). These limitations of fixed-SST experiments on the simulation of rainfall in areas impacted by the Indian Ocean clearly extend to our discussion of droughts and pluvials in these regions. Further research on drought occurrence in the areas surrounding the Indian Ocean should be conducted with a fully coupled ocean model.

The increase in drought frequency in response to the trend pattern (Fig. 11a) is largely consistent with the work of Kumar et al. (2004), which showed an increase in SSTs over the years 1950–2000, accompanied by a decreasing trend in land-only precipitation. Similarly, Li et al. (2008) show that SST forcing, primarily from the tropics, is able to induce most of the observed weakening of the East Asian summer monsoon observed between 1950 and 2000.

The analysis of Vecchi and Soden (2007) and Vecchi et al. (2008) showed significant dependence of the SST trend pattern on the original SST dataset. They show that the cooling along the equator in the eastern Pacific shown in Fig. 1b, derived from Hadley Centre data, is not present in the SST trend pattern derived from the Smith and Reynolds (2004) dataset. This is an indication that not all features of the SST trend pattern may be robust and that drought and pluvial results from these experiments forced with the Hadley-based trend patterns may differ from experiments forced by different SST trend patterns.

6. Conclusions

Climate model simulations run as part of the CLIVAR Drought Working Group initiative were analyzed to determine the impact of three SST anomaly patterns on drought and pluvial frequency and intensity around the world. The three patterns are a global pattern reflecting the observed warming trend, a Pacific pattern, and an Atlantic pattern. Five different atmospheric models (GFDL, NSIPP, CAM3.5, CCM3, and GFS) were coupled to fixed-SST oceans to test the impact of these SST anomalies on droughts and pluvials relative to a climatologically forced control run.

The five models generally yield similar results in the locations of droughts and pluvials. In all of the simulations, areas with an increase (decrease) in the mean drought index values tend to also show an increase in the frequency of high-end (low end) extreme drought index values. Additionally, areas with more frequent extremes also tend to show higher intensity extremes. Though all models are in general agreement with the MMM in broad terms, CAM3.5 tends to be more sensitive than the other models in Africa, and peak values of drought and pluvial frequency tend to be higher with CAM3.5 and lower with GFS than with the other models.

Areas of greatest drought and pluvial sensitivity under these forcing scenarios include most of the Americas. MMM results show that drought frequencies are highest in the continental United States, Mexico, and southern South America when the Pacific is cold and the Atlantic is warm (PcAw). Pluvial frequencies in these regions are highest with the opposite oceanic forcings (PwAc). Southern Central America and northern South America respond in the opposite way to these forcings, with drought maximized in PwAc experiments and pluvials maximized in PcAw experiments. Indonesia is strongly affected by Pacific conditions, with a cold Pacific pattern (which actually includes warming in the ocean area surrounding Indonesia; see Fig. 1c) yielding increases in pluvials and a warm Pacific pattern yielding increases in

droughts. More modest impacts are seen in Europe and Australia, with Australia following Indonesia's patterns but with substantially reduced frequencies. The largest areas of modest impact in Europe occur with increased droughts in PcAc and increased pluvials in PwAw. Results for areas strongly impacted by Indian Ocean SSTs should be interpreted with caution given the importance of ocean–atmosphere feedbacks in this region and the limitations of fixed-SST experiments.

These idealized experiments are a useful aid to improve our understanding of the factors contributing to drought in regions all around the world; however, it is important to remember that these experiments are indeed idealizations and not perfect reflections of the real world. Nevertheless, the substantial agreement between these five very different models on the locations of increased drought and pluvial frequency under each of the experimental scenarios indicates that these results are likely to be robust.

Acknowledgments. This work was carried out as part of a U.S. CLIVAR Drought Working Group activity supported by NASA, NOAA, and NSF to coordinate and compare climate model simulations forced with a common set of idealized SST patterns. The authors thank NASA's Global Modeling and Assimilation Office (GMAO) for making the NSIPP1 runs available, the Lamont-Doherty Earth Observatory of Columbia University for making their CCM3 runs available, NOAA's Climate Prediction Center (CPC)/Climate Test Bed (CTB) for making the GFS runs available, NOAA's Geophysical Fluid Dynamics Laboratory (GFDL) for making the AM2.1 runs available, the National Center for Atmospheric Research (NCAR) for making the CAM3.5 runs available, and the Center for Ocean Land Atmosphere (COLA) and the University of Miami's Rosenstiel School of Marine and Atmospheric Science for making the CCSM3.0 coupled model runs available. We would also like to thank Yana Malysheva for guaranteeing that the GFDL data were consistent with the CMOR protocol, and Paul Ginoux, Gabriel Vecchi, and four anonymous reviewers for their helpful comments on the manuscript.

REFERENCES

Alley, W. M., 1984: The Palmer Drought Severity Index: Limitations and assumptions. *J. Climate Appl. Meteor.,* **23,** 1100–1109.

Bacmeister, J., P. J. Pegion, S. D. Schubert, and M. J. Suarez, 2000: An atlas of seasonal means simulated by the NSIPP 1 atmospheric GCM. Vol. 17, NASA Tech. Memo. 104606, Goddard Space Flight Center, Greenbelt, MD, 194 pp.

Bracco, A., F. Kucharski, F. Molteni, W. Hazeleger, and C. Severijns, 2007: A recipe for simulating the interannual variability of the Asian summer monsoon and its relation with ENSO. *Climate Dyn.,* **28,** 441–460.

Cai, W., P. H. Whetton, and A. B. Pittock, 2001: Fluctuations of the relationship between ENSO and northeast Australian rainfall. *Climate Dyn.,* **17,** 421–432.

Campana, K., and P. Caplan, Eds., cited 2005: Technical procedures bulletin for T382 Global Forecast System. [Available online at http://www.emc.ncep.noaa.gov/gc_wmb/Documentation/TPBoct05/T382.TPB.FINAL.htm.]

Campbell, G. S., and J. M. Norman, 1998: *An Introduction to Environmental Biophysics*. 2nd ed. Springer-Verlag, 286 pp.

Delworth, T. L., and Coauthors, 2006: GFDL's CM2 global coupled climate models. Part I: Formulation and simulation characteristics. *J. Climate,* **19,** 643–674.

Dingman, S. L., 1994: *Physical Hydrology*. Prentice-Hall, 600 pp.

Enfield, D. B., and E. J. Alfaro, 1999: The dependence of Caribbean rainfall on the interaction of the tropical Atlantic and Pacific Oceans. *J. Climate,* **12,** 2093–2103.

——, A. M. Mestas-Nunez, and P. J. Trimble, 2001: The Atlantic multidecadal oscillation and its relation to rainfall and river flows in the continental U.S. *Geophys. Res. Lett.,* **28,** 2077–2080.

England, M. H., C. C. Ummenhofer, and A. Santoso, 2006: Interannual rainfall extremes over southwest Western Australia linked to Indian Ocean climate variability. *J. Climate,* **19,** 1948–1969.

Findell, K. L., T. R. Knutson, and P. C. D. Milly, 2006: Weak simulated extratropical responses to complete tropical deforestation. *J. Climate,* **19,** 2835–2850.

Fontaine, B., and S. Janicot, 1996: Sea surface temperature fields associated with West African rainfall anomaly types. *J. Climate,* **9,** 2935–2940.

GFDL Global Atmospheric Model Development Team, 2004: The new GFDL global atmosphere and land model AM2–LM2: Evaluation with prescribed SST simulations. *J. Climate,* **17,** 4641–4673.

Giannini, A., J. C. H. Chiang, M. A. Cane, Y. Kushnir, and R. Seager, 2001: The ENSO teleconnection to the tropical Atlantic Ocean: Contributions of the remote and local SSTs to rainfall variability in the tropical Americas. *J. Climate,* **14,** 4530–4544.

——, R. Saravanan, and P. Chang, 2003: Oceanic forcing of Sahel rainfall on interannual to interdecadal time scales. *Science,* **302,** 1027–1030.

Gibbs, W. J., and J. V. Maher, 1967: Rainfall deciles as drought indicators. Australian Bureau of Meteorology Bulletin 48, 33 pp.

Hastenrath, S., 1978: On modes of tropical circulation and climate anomalies. *J. Atmos. Sci.,* **35,** 2222–2231.

Heim, R. R., Jr., 2002: A review of twentieth-century drought indices used in the United States. *Bull. Amer. Meteor. Soc.,* **83,** 1149–1165.

Held, I. M., T. L. Delworth, J. Lu, K. L. Findell, and T. R. Knutson, 2005: Simulation of Sahel drought in the 20th and 21st centuries. *Proc. Natl. Acad. Sci. USA,* **102,** 17 891–17 896.

Hendon, H. H., 2003: Indonesian rainfall variability: Impacts of ENSO and local air–sea interaction. *J. Climate,* **16,** 1775–1790.

Herweijer, C., and R. Seager, 2008: The global footprint of persistent extra-tropical drought in the instrumental era. *Int. J. Climatol.,* **28,** 1761–1774, doi:10.1002/joc.1590.

Hoerling, M., and A. Kumar, 2003: The perfect ocean for drought. *Science,* **299,** 691–694.

——, J. Hurrell, J. Eischeid, and A. Phillips, 2006: Detection and attribution of twentieth-century northern and southern African rainfall change. *J. Climate,* **19,** 3989–4008.

Kaiser, H. F., 1958: The varimax criterion for analytic rotation in factor analysis. *Psychometrika,* **23,** 187–200, doi:10.1007/BF02289233.

Kerr, R. A., 2000: A North Atlantic climate pacemaker for the centuries. *Science,* **288,** 1984–1986.

Keyantash, J., and J. A. Dracup, 2002: The quantification of drought: An evaluation of drought indices. *Bull. Amer. Meteor. Soc.,* **83,** 1167–1180.

Kiehl, J. T., J. J. Hack, G. Bonan, B. A. Boville, D. L. Williamson, and P. J. Rasch, 1998: The National Center for Atmospheric Research Community Climate Model: CCM3. *J. Climate,* **11,** 1131–1149.

Kumar, A., F. Yang, L. Goddard, and S. Schubert, 2004: Differing trends in the tropical surface temperatures and precipitation over land and oceans. *J. Climate,* **17,** 653–664.

Lau, N.-C., and M. J. Nath, 2000: Impact of ENSO on the variability of the Asian–Australian monsoons as simulated in GCM experiments. *J. Climate,* **13,** 4287–4309.

Li, H., A. Dai, T. Zhou, and J. Lu, 2008: Responses of East Asian summer monsoon to historical SST and atmospheric forcing during 1950–2000. *Climate Dyn.,* doi:10.1007/s00382-008-0482-7.

McCabe, G. J., M. A. Palecki, and J. L. Betancourt, 2004: Pacific and Atlantic Ocean influences on multidecadal drought frequency in the United States. *Proc. Natl. Acad. Sci. USA,* **101,** 4136–4141.

Milly, P. C. D., and A. B. Shmakin, 2002: Global modeling of land water and energy balances. Part I: The Land Dynamics (LaD) model. *J. Hydrometeor.,* **3,** 283–299.

Mo, K. C., and M. Chelliah, 2006: The modified Palmer drought severity index based on the NCEP North American Regional Reanalysis. *J. Appl. Meteor. Climatol.,* **45,** 1362–1375.

Neale, R. B., J. H. Richter, and M. Jochum, 2008: The impact of convection on ENSO: From a delayed oscillator to a series of events. *J. Climate,* **21,** 5904–5924.

Oleson, K. W., and Coauthors, 2008: Improvements to the Community Land Model and their impact on the hydrological cycle. *J. Geophys. Res.,* **113,** G01021, doi:10.1029/2007JG000563.

Palmer, W., 1965: Meteorological drought. Research Paper 45, U.S. Weather Bureau, Washington, D.C., 58 pp.

Priestley, C. H. S., and R. J. Taylor, 1972: On the assessment of surface heat flux and evaporation using large-scale parameters. *Mon. Wea. Rev.,* **100,** 81–92.

Rayner, N. A., D. E. Parker, E. B. Horton, C. K. Folland, L. V. Alexander, D. P. Rowell, E. C. Kent, and A. Kaplan, 2003: Global analyses of sea surface temperature, sea ice, and night marine air temperature since the late nineteenth century. *J. Geophys. Res.,* **108,** 4407, doi:10.1029/2002JD002670.

Rind, D., R. Goldberg, J. Hansen, C. Rosenzweig, and R. Ruedy, 1990: Potential evapotranspiration and the likelihood of future drought. *J. Geophys. Res.,* **95** (D7), 9983–10 004.

Rogers, R. R., and M. K. Yau, 1989: *A Short Course in Cloud Physics*. 3rd ed. Elsevier Science, 304 pp.

Schubert, S. D., M. J. Suarez, P. J. Pegion, R. D. Koster, and J. T. Bacmeister, 2004: On the cause of the 1930s Dust Bowl. *Science,* **303,** 1855–1859.

——, and Coauthors, 2009: A U.S. CLIVAR project to assess and compare the responses of global climate models to drought-related SST forcing patterns: Overview and results. *J. Climate,* **22,** 5251–5272.

Seager, R., N. Harnik, Y. Kushnir, W. Robinson, and J. Miller, 2003: Mechanisms of hemispherically symmetric climate variability. *J. Climate,* **16,** 2960–2978.

——, Y. Kushnir, C. Herweijer, N. Naik, and J. Velez, 2005: Modeling tropical forcing of persistent droughts and pluvials: 1856–2000. *J. Climate,* **18,** 4068–4091.

Shabbar, A., and W. Skinner, 2004: Summer drought patterns in Canada and the relationship to global sea surface temperatures. *J. Climate,* **17,** 2866–2880.

Smith, T. M., and R. W. Reynolds, 2004: Improved extended reconstruction of SST (1854–1997). *J. Climate,* **17,** 2466–2477.

Stöckli, R., and Coauthors, 2008: Use of FLUXNET in the Community Land Model development. *J. Geophys. Res.,* **113,** G01025, doi:10.1029/2007JG000562.

Suppiah, R., 2004: Trends in the Southern Oscillation phenomenon and Australian rainfall and changes in their relationship. *Int. J. Climatol.,* **24,** 269–290.

Sutton, R. T., and D. L. R. Hodson, 2005: Atlantic Ocean forcing of North American and European summer climate. *Science,* **309,** 115–118.

Svoboda, M., and Coauthors, 2002: The Drought Monitor. *Bull. Amer. Meteor. Soc.,* **83,** 1181–1190.

Thornthwaite, C. W., 1948: An approach toward a rational classification of climate. *Geogr. Rev.,* **38,** 55–94.

Vecchi, G. A., and B. J. Soden, 2007: Global warming and the weakening of the tropical circulation. *J. Climate,* **20,** 4316–4340.

——, A. Clement, and B. J. Soden, 2008: Examining the tropical Pacific's response to global warming. *EOS, Trans. Amer. Geophys. Union,* **89,** doi:10.1029/2008EO090002.

Von Storch, H., and F. W. Zwiers, 1999: *Statistical Analysis in Climate Research*. Cambridge University Press, 484 pp.

Wang, B., Q. Ding, X. Fu, I.-S. Kang, K. Jin, J. Shukla, and F. Doblas-Reyes, 2005: Fundamental challenge in simulation and prediction of summer monsoon rainfall. *Geophys. Res. Lett.,* **32,** L15711, doi:10.1029/2005GL022734.

Wells, N., S. Goddard, and M. J. Hayes, 2004: A self-calibrating Palmer drought severity index. *J. Climate,* **17,** 2335–2351.

White, D. H., and B. O'Meagher, 1995: Coping with exceptional droughts in Australia. *Drought Network News,* No. 7, National Drought Mitigation Center, Lincoln, NE, 13–17.

Wilhite, D. A., and M. H. Glanz, 1985: Understanding the drought phenomenon: The role of definitions. *Water Int.,* **10,** 111–120.

Xin, X., R. Yu, T. Zhou, and B. Wang, 2006: Drought in late spring of south China in recent decades. *J. Climate,* **19,** 3197–3206.

Zhou, T., and Coauthors, 2008: The CLIVAR C20C project: Which components of the Asian–Australian monsoon circulation variations are forced and reproducible? *Climate Dyn.,* **33,** 1051–1068, doi:10.1007/s00382-008-0501-8.